Vol. 677: 177–196, 2021
https://doi.org/10.3354/meps13852

MARINE ECOLOGY PROGRESS SERIES
Mar Ecol Prog Ser

Published October 28

Bottom temperature warming and its impact on demersal fish off the Pacific coast of northeastern Japan

Shigeho Kakehi[1,*], Yoji Narimatsu[2], Yuriko Okamura[3], Asagi Yagura[3], Shin-ichi Ito[4]

[1]Shiogama Field Station, Fisheries Stock Assessment Center, Fisheries Resources Institute, Japan Fisheries Research and Education Agency, Shinhama-cho, Shiogama, Miyagi 985-0001, Japan
[2]Hachinohe Field Station, Fisheries Stock Assessment Center, Fisheries Resources Institute, Japan Fisheries Research and Education Agency, Shimomekurakubo, Same, Hachinohe, Aomori 031-0841, Japan
[3]Miyagi Prefecture Fisheries Technology Institute, Watanoha, Sodenohama, Ishinomaki, Miyagi 986-2135, Japan
[4]Atmosphere and Ocean Research Institute, The University of Tokyo, Kashiwanoha, Kashiwa, Chiba 277-8564, Japan

ABSTRACT: Global climate change occurs not only at the ocean surface but also at the ocean bottom, which is the main habitat of demersal fish. To clarify the current status of bottom temperature warming off the Pacific coast of northeastern Japan, we examined gridded bottom temperature fields from 2003 to 2019. These fields were created by a newly developed gridding method using flexible Gaussian filter weighting with time, distance, and depth. Spatially averaged bottom temperature had a strong, significant warming trend of 0.083 to 0.115°C yr^{-1} in depth zones of 150–300 m, indicating bottom temperature warming. Corresponding to the warming, increases in landing amounts were found for warm-water species such as searobin in the middle region of our study area (37° 50′–39° N). Seasonal catch amounts suggest that ribbon fish and swimming crab recently began to overwinter and reproduce in the area. The distribution shifts of non-target species in fisheries were also analyzed using bottom otter trawl survey data from the area from 2003 to 2019. Northward distribution shifts and increases in density were observed in blackbelly lantern shark and bighand grenadier, indicating that bottom temperature warming led to habitat expansion. Conversely, darkfin sculpin and jelly eelpout shifted northward with decreasing density, suggesting that bottom temperature warming had a negative effect on them. Deepsea bonefish shifted deeper into colder waters with increasing density and mean body weight. Thus, changes and responses of demersal fish to bottom temperature warming in the area were revealed.

KEY WORDS: Flexible Gaussian filter · Bottom temperature field · Bottom temperature warming · Demersal fish catch · Demersal fish distribution · Northeastern Japan

1. INTRODUCTION

There is unequivocal evidence for ocean warming in the upper ocean (IPCC 2014). Many studies suggest that ocean warming has a significant impact on marine ecosystems (e.g. Hoegh-Guldberg & Bruno 2010, Doney et al. 2012). Marine ecosystems generally respond to ocean warming through distribution shifts to higher latitudes and deeper waters (Perry et al. 2005, Cheung et al. 2013). The shifts in marine fishes and invertebrates from ocean warming affect fisheries (Free et al. 2019). Fishery production typically consists not only of the dominant small pelagic species but also of many kinds of demersal species.

*Corresponding author: kakehi@affrc.go.jp

In contrast to pelagic species that migrate widely, demersal fish tend to be distributed in relatively limited and specific depth zones, the so-called depth zonation (Fujita et al. 1995, King et al. 2006, Menezes et al. 2006). Therefore, changes in the bottom temperature in the optimum depth zone strongly influence the distribution and density of demersal fish. Because the extent of the influence is different among species, a description of the impact of bottom temperature warming on each species is essential.

The area off the Pacific coast of northeastern Japan (Fig. 1a) is one of the world's most productive fishing grounds. In this area, the warm Kuroshio Extension and Tsugaru Warm Current, and the cold Oyashio Current meet and mix (Kawai 1972, Hanawa & Mitsudera 1986), resulting in high primary production. Owing to the nature of these oceanic currents, various fishes originating from cold and warm waters have been caught in the area. The variability in oceanic conditions strongly influences the fisheries. The return rate of adult chum salmon *Oncorhynchus keta* decreased when the frequency of warm waters in the coastal areas increased (Wagawa et al. 2016). The amount of landed North Pacific krill *Euphausia pacifica* decreased under warmer oceanographic conditions (Endo 2000). This area is also an important fishery ground for demersal fish (Fujita et al. 1993). Okamura et al. (2021) reported that the catch of warm-water species such as ribbon fish *Trichiurus lepturus* and swordtip squid *Uroteuthis edulis* have recently increased. The Japan Meteorological Agency reported that the sea surface temperature in the area has had a strong, significant warming trend ($p < 0.01$) of 0.76°C per 100 yr (https://www.data.jma.go.jp/gmd/kaiyou/data/shindan/a_1/japan_warm/japan_warm.html, last accessed 9 Mar 2021). Although this report supports the increase in the catch of warm-water species, for demersal fish, the bottom temperature, rather than the sea surface temperature, is a key factor controlling their geographical distribution. However, the current status of warming of the bottom temperature in the area has not been clarified.

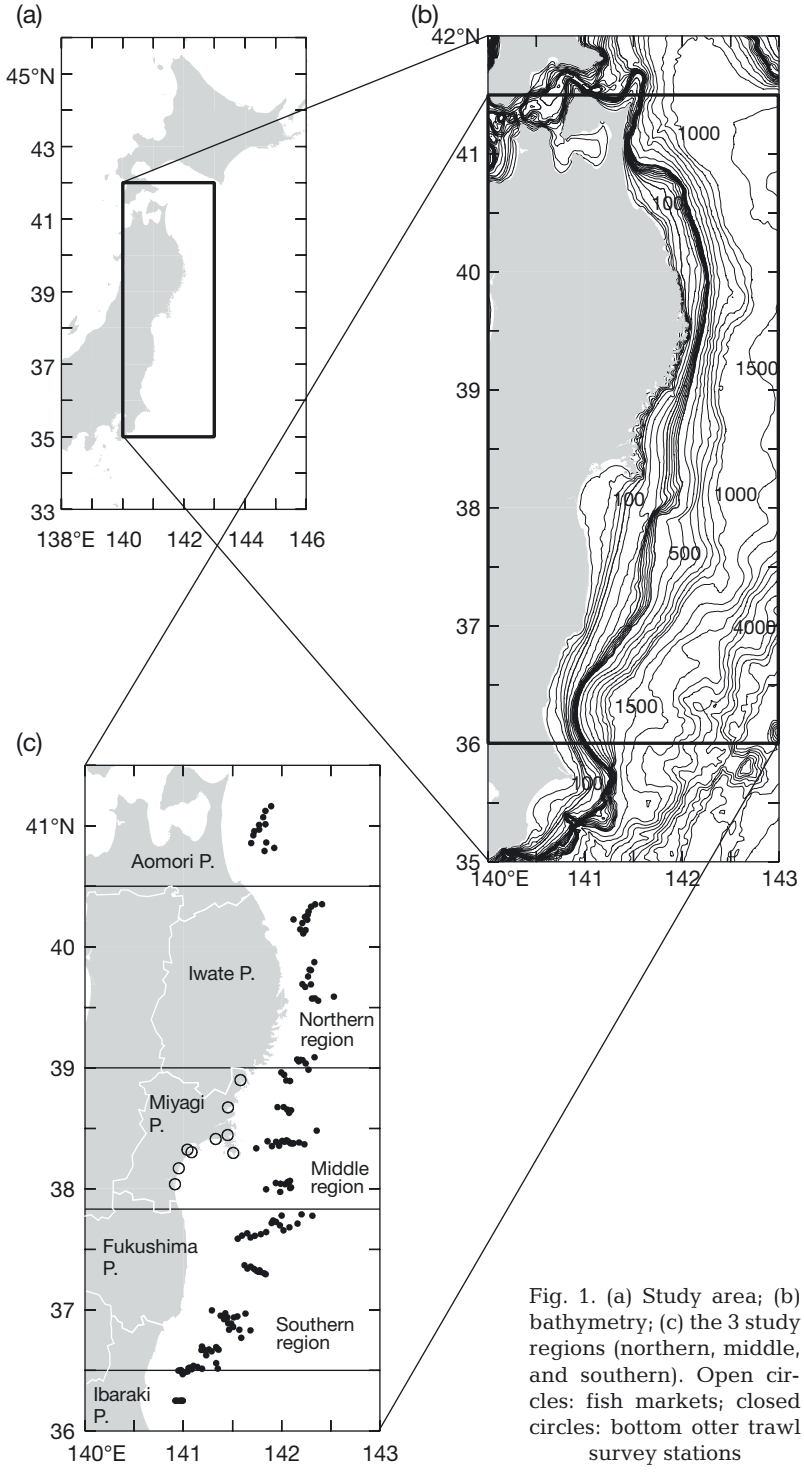

Fig. 1. (a) Study area; (b) bathymetry; (c) the 3 study regions (northern, middle, and southern). Open circles: fish markets; closed circles: bottom otter trawl survey stations

To analyze the relationship between bottom temperature warming and the distribution and density of demersal fish, bottom temperature data must be

prepared. Calculating the bottom temperature using the ocean circulation model is one method (Weinert et al. 2016); however, the bias between the model and observation should be considered (Kuroda et al. 2017). For a direct comparison between the modeled bottom temperature and the optimum temperature for fish, the bias should be accurately determined. To do so, observation of the bottom temperature is first needed. In general, the bottom temperature data observed during fish sampling are used (Sedberry & Van Dolah 1984). Alternatively, hydrographic observational data independent of fish sampling at standard depths, such as at a depth of 100 m, are also used for analysis (Tian et al. 2011). Owing to the depth zonation in the demersal fish distribution, as mentioned above, the bottom temperature for each depth zone, such as 50–300 m with 50 m increments, should be estimated. However, temperature measurements tend to be biased toward certain depth zones, and typically do not cover all depth zones. In particular, the bathymetry in the area is generally steep (Fig. 1b). To obtain the bottom temperature in 50 m depth increments, measurements at horizontal intervals of 5–10 km are needed orthogonal to the isobathymetric lines. Because actual observations at such a high spatial resolution are impractical, it may not be possible to obtain bottom temperature data for all zones. Therefore, a method is needed with which a bottom temperature field can be created through interpolation.

Shimizu & Ito (1996) proposed a method for creating monthly temperature fields at a standard depth using a flexible Gaussian interpolation based on observed temperature data. The temperature distributions created by this method are publicly available on the website of the Japan Fisheries Research and Education Agency (https://ocean.fra.go.jp/temp/temp.html, last accessed 9 Mar 2021) and the data have been used to analyze water mass and fish distributions (Ito 2001, Katayama et al. 2004). For our objective, the method had to be extended to measurements of the bottom temperature.

In this study, we propose a new method for creating a monthly bottom temperature field based on observational data using a flexible Gaussian interpolation. By applying this method, we create monthly bottom temperature fields off the Pacific coast of northeastern Japan from 2003 to 2019. Using the fields, we analyze the trend of the bottom temperature at depths of 50–300 m in 50 m increments. We also analyze the relationship between bottom temperature warming and the catch and distribution of demersal fish within the area. These data provide a useful description of the actual status of bottom temperature warming in the area and its impact on demersal fish.

2. MATERIALS AND METHODS

2.1. Preparation of bottom temperature data

Temperature data were obtained from the Fishery Resource Conservation System (FRESCO, https://www.fresco.jafic.or.jp/, last accessed 9 Mar 2021), which is a database operated by the Fisheries Agency of Japan. Profiles of temperature and salinity using conductivity-temperature-depth sensors (CTD) measured by research vessels of the Fisheries Agency of Japan, the Japan Fisheries Research and Education Agency, and the public fishery research institutes are archived in the database. Temperature profiles off the Pacific coast of northeastern Japan (34°–42° N, 140°–143° E) from 2000 to 2019 were downloaded. When the deepest measurement of each profile was greater than 50 m and within 30% of the bottom depth above the sea floor (for example, ≥70 m at a bottom depth of 100 m), the temperature at the deepest measurement was adopted as the bottom temperature. The bottom depth data were based on 500 m mesh bottom depth data (J-EGG500; JODC-Expert Grid data for Geography) provided by the Japan Ocean Data Center (JODC, https://www.jodc.go.jp/jodcweb/index_j.html, last accessed 9 Mar 2021). Because the J-EGG500 is not based on the latitude/longitude coordinate system, we created 0.5′ latitude × 0.5′ longitude mesh bottom depth data interpolating the J-EGG500 through inverse distance weighting. Because the number of adopted bottom temperatures in each month was significantly lower (mean ± SD: 43.5 ± 11.6) from 2000 to 2002 than after 2003 (83.4 ± 40.5) ($p < 0.01$; Student's *t*-test), bottom temperature data from 2003 to 2019 were used for further analysis.

2.2. Flexible Gaussian interpolation method

Shimizu & Ito (1996) proposed a flexible Gaussian interpolation method to generate a gridded temperature field from randomly distributed observational temperature data. The gridded temperature (T) at a grid point (i, j) is calculated as follows:

$$T(i,j) = \frac{\sum_{k=1}^{N(i,j)} T_k \exp\left\{-\left[\left(\frac{d_k}{D(i,j)}\right)^2 + \left(\frac{\tau_k}{\tau_0}\right)^2\right]\right\}}{\sum_{k=1}^{N(i,j)} \exp\left\{-\left[\left(\frac{d_k}{D(i,j)}\right)^2 + \left(\frac{\tau_k}{\tau_0}\right)^2\right]\right\}} \quad (1)$$

where $N(i,j)$ is the number of observations within an interpolation circle (details in Section 2.3), T_k is the observed temperature, d_k is the distance between the center of the interpolation circle and the location of the observation, τ_k is the time difference between the center of the interpolation time and the date of the observation, $D(i,j)$ is the spatial interpolation scale, and τ_0 is the temporal interpolation scale. In a flexible Gaussian interpolation, $D(i,j)$ is denoted as a function of the number of observations ($N(i,j)$) as follows:

$$D(i,j) = D_{\max} - (D_{\max} - D_{\min})\left[1 - \exp\left(-\frac{N(i,j)}{N_0}\right)\right] \quad (2)$$

where $D_{\min}$ and $D_{\max}$ are the minimum and maximum values of the spatial interpolation scale, respectively, and N_0 is the scale coefficient. Shimizu & Ito (1996) presented realistic values for $D_{\min}$, $D_{\max}$, N_0, and τ_0 in the study area as 10 km, 40 km, 200, and 10 days, respectively. Our study also used these values.

This method was developed to create a temperature field at an isobaric layer. In this study, we need a temperature field along the bottom; therefore, we modified Eq. (1) by adding the effect of the difference in depth between the center of the interpolation circle and the location of the observation. The modified gridded temperature (T_m) at grid point (i,j) is:

$$T_m(i,j) = \frac{\sum_{k=1}^{N(i,j)} T_k \exp\left\{-\left[\left(\frac{d_k}{D(i,j)}\right)^2 + \left(\frac{\tau_k}{\tau_0}\right)^2 + \left(\frac{Z_k}{Z_0}\right)^2\right]\right\}}{\sum_{k=1}^{N(i,j)} \exp\left\{-\left[\left(\frac{d_k}{D(i,j)}\right)^2 + \left(\frac{\tau_k}{\tau_0}\right)^2 + \left(\frac{Z_k}{Z_0}\right)^2\right]\right\}} \quad (3)$$

where Z_k is the difference in depth between the center of the interpolation circle and the location of the observation, and Z_0 is the interpolation scale for depth. To calculate Z_k, our 0.5′ latitude × 0.5′ longitude mesh bottom depth data mentioned above were used. To determine an optimal value for Z_0, we assessed the estimation error using a sensitivity analysis as follows. For the measurement of the bottom temperature, an interpolated value (T'_m) was calculated using Eq. (3) setting the center of the interpolation circle as the location of the observation and the center of the interpolation time as the date of the observation. When calculating T'_m, the temperature at the center of the interpolation circle (T_c), that is, the temperature of the targeted observation, was excluded (Fig. S1 in the Supplement at www.int-res.com/articles/suppl/m677p177_supp.pdf). For all measurements of the bottom temperature, T'_m was calculated by giving a Z_0 of 10–60 m in 10 m increments. The root-mean-square differences between T'_m and T_c for each Z_0 were estimated and used to assess the optimal Z_0. To evaluate the performance of our new interpolation method (Eq. 3), we compared the root-mean-square differences obtained using Eqs. (1) & (3). We also compared the root-mean-square differences obtained from the Gaussian interpolation weighting with distance (T_g) and the inverse distance interpolation (T_i). The Gaussian interpolation weighting with distance is denoted as:

$$T_g = \frac{\sum_{k=1}^{n} T_k \exp\left[-\left(\frac{d_k}{d_0}\right)^2\right]}{\sum_{k=1}^{n} \exp\left[-\left(\frac{d_k}{d_0}\right)^2\right]} \quad (4)$$

where n is the number of observations within an interpolation circle and d_0 is the spatial interpolation scale. The d_0 was set to 25 km, which corresponds to the average between $D_{\min}$ and $D_{\max}$. The inverse distance interpolation is denoted as follows:

$$T_i = \frac{\sum_{k=1}^{n} \frac{T_k}{d_k}}{\sum_{k=1}^{n} \frac{1}{d_k}} \quad (5)$$

To evaluate the accuracy of the estimation, we calculated the determination coefficient (r^2) between the estimation (T'_m) and the observation (T_c).

2.3. Monthly bottom temperature field

Monthly bottom temperature fields off the Pacific coast of northeastern Japan from 2003 to 2019 were created using Eq. (3) incorporating the optimal Z_0. The gridded area was 35°–42° N, 140°–143° E, considering the spatial interpolation scale $D(i,j)$. The horizontal resolution was 1′ latitude × 1′ longitude and the radius of the interpolation circle was 55 km (= 30′ latitude). Bottom temperature measurements included within the interpolation circle were used for the interpolation. The center of the interpolation time was set to the middle date of each month: the 14th for February and the 15th for other months. A grid point with fewer than 5 measurements in the interpolation circle was treated as missing. When all depths of the bottom temperature within an interpolation circle

were shallower or deeper than the depth of the center of the circle, we treated the temperature of the grid as missing, avoiding extrapolation.

To examine the bottom temperature trend, the spatially averaged bottom temperature in the depth zone was estimated using the gridded monthly bottom temperature field. The study area was divided into 3 regions: southern (36° 30′–37° 50′ N), middle (37° 50′–39° N), and northern (39°–40° 30′ N) regions, considering the prefecture borders for comparison with fish landings (Fig. 1c). The spatially averaged bottom temperatures in each region in the depth zones of 50–100, 100–150, 150–200, 200–250, and 250–300 m from 2003 to 2019 were estimated monthly. The trend of the bottom temperature was calculated by linear regression using the least-squares method. The slope of the trend was tested through a parametric test using Pearson's product-moment correlation coefficient. The parametric test for the slope of the trend was performed using the TDIST function in Microsoft Excel 365, and the alpha value for statistical significance was set at 5%.

2.4. Demersal fish data for analyzing interannual variation

Catch data for demersal fish from 2003 to 2019 in Miyagi Prefecture, located in the middle region of our study area, were extracted from the Comprehensive Fishery Information System for MIYAGI, which are fishery statistics compiled by the prefecture. The numbers of fish landed in 9 fish markets in the prefecture (open circles in Fig. 1c) were analyzed. These 9 markets account for almost all landings in the prefecture. Reasons for choosing the data of the prefecture were as follows: (1) Fishery production in the prefecture is the largest in our study area (4th in Japan in 2019; Ministry of Agriculture, Forestry and Fisheries 2021). (2) Fishery operations in the southern region of the area, mainly Fukushima Prefecture, decreased after 2011 due to the Great East Japan Earthquake and tsunami, and the subsequent Fukushima Dai-ichi Nuclear Power Plant (FDNPP) accident that occurred on and after March 11, 2011 (Wada et al. 2013, 2016, Shibata et al. 2017). (3) There are slightly more missing values in the spatially averaged bottom temperature in the northern region of the area (details in Section 3.3). We analyzed catch data for Japanese flounder *Paralichthys olivaceus*, Pacific cod *Gadus microcephalus*, ribbon fish *Trichiurus lepturus*, searobin *Lepidotrigla microptera*, common octopus *Octopus sinensis*, Japanese flying squid *Todarodes pacificus*, spear squid *Heterololigo bleekeri*, and swimming crab *Portunus trituberculatus*. We chose these species because some obvious changes in catch were observed during our study period. These species also have high catches and commercial value. The fraction of the catches of these 8 species to the total catch, and the fraction to the total catch of demersal fish, accounted for 3.5% and 54.3%, respectively, in 2019. These catch data represent the catch within the prefecture because landed demersal fish in these markets come from fleets that are permitted by the governor of the prefecture to catch demersal fish off the prefecture. For the searobin catch, only data from the largest fish market (Ishinomaki, located at 38° 24.8′ N, 141° 19.8′ E) were used because of the small catch traded in the other markets. Kawabata et al. (2006) reported that Japanese flying squid were distributed near the bottom of the continental shelf at 300–600 m depth in the daytime. Spear squid also stay near the sea floor during the daytime. Indeed, Tian et al. (2011) treated spear squid as demersal fish because they were caught by bottom trawl fisheries. These 2 squid species are also caught by bottom trawl off Miyagi prefecture during the daytime when they stay near the sea floor. Thus, the distributions of both squids are considered to be influenced by the bottom temperature; therefore, we included their catch data in this study. The characteristics of the habitat preferences for these species are shown in Table 1. Catch data were summed seasonally, i.e. winter (January–March), spring (April–June), summer (July–September), and autumn (October–December).

For demersal fish data independent of fisheries, we used fish samples collected from bottom otter trawl surveys by the R/V 'Wakataka-maru' of the Japan Fisheries Research and Education Agency from 2003 to 2019 (Hattori et al. 2008, 2010, Narimatsu et al. 2017). The surveys were conducted at depths of 150–900 m at 36°–41° 30′ N. The tow of the trawl was conducted at approximately 150 stations during October–November every year (closed circles in Fig. 1c). The trawl net had a total length of 44.1 m and a mouth width of 5.4 m. The net was composed of a mesh size of 50 mm and a cover net with an 8 mm mesh at the codend. All tows were conducted during daytime. The net was towed along an isobathymetric line at an average ship speed of 80–110 m min^{-1} for 30 min. The arrival and departure of the net on the bottom, and the opening width of the net were measured using the Otter and Net Recorder system (Furuno Electric Co.). The positions of the arrival and departure of the net on the bottom were recorded

Table 1. Species included in this study

Common name	Species name	Geographic affinity	Habitat in Japan	Depth (m)	Reference
Japanese flounder	*Paralichthys olivaceus*	Warm	Entire coastal area	30–180	Nakabo & Doiuchi (2013a)
Pacific cod	*Gadus microcephalus*	Cold	Northern part (>36° N)	40–550	Mishima (1984), Narimatsu et al. (2015)
Ribbon fish	*Trichiurus lepturus*	Warm	Entire coastal area	100–350	Nakabo & Doiuchi (2013b)
Searobin	*Lepidotrigla microptera*	Warm	Entire coastal area	20–340	Yamada & Yagishita (2013)
Common octopus	*Octopus sinensis*	Warm	Entire coastal area	<100	Norman et al. (2014)
Japanese flying squid	*Todarodes pacificus*	Broad	Entire coastal area	<600	Kawabata et al. (2006)
Spear squid	*Heterololigo bleekeri*	Warm	Entire coastal area	<150	Jereb & Roper (2010)
Swimming crab	*Portunus trituberculatus*	Warm	Entire coastal area	<100	Miyake (1991)
Blackbelly lantern shark	*Etmopterus lucifer*	Warm	Entire coastal area	158–1357	Ebert et al. (2013)
Bighand grenadier	*Abyssicola macrochir*	Warm	Entire coastal area	Predominant at 300–500 m	Fujiwara et al. (2005)
Deepsea bonefish	*Pterothrissus gissu*	Warm	Entire coastal area	Predominant at 500 m	Aguzzi et al. (2018)
Darkfin sculpin	*Malacocottus zonurus*	Cold	Northern part (>36° N)	140–500	Glubokov et al. (2019)
Jelly eelpout	*Bothrocara tanakae*	Cold	Northern part (>36° N)	274–892	Anderson et al. (2009)

using GPS. The area swept by the trawl was estimated by multiplying the net-opening width with the tow distance.

To remove the recent decrease in fishery pressure in the above-mentioned southern region, we analyzed the non-target species in the fisheries: blackbelly lantern shark *Etmopterus lucifer*, bighand grenadier *Abyssicola macrochir*, deepsea bonefish *Pterothrissus gissu*, darkfin sculpin *Malacocottus zonurus*, and jelly eelpout *Bothrocara tanakae*. These 5 species accounted for 95.6% of the total catch of the non-target species in the fisheries during our study period. The main habitats of these species partially overlap with the distribution range of Pacific cod, a commercially important species; however, the areas where blackbelly lantern shark and bighand grenadier are bycatch are avoided by fishermen because shark skin and spiny scales damage the main target species, resulting in a reduction in commercial value. For the other 3 species examined, the impact of bycatch from the commercial fishery is unknown; however, conducting fishery operations in the major distribution area of these species is considered to be inefficient because it forces fishermen to extract only a few target species from a large number of non-target fish. Therefore, we assumed that the impact of bycatch on these species in commercial fisheries was negligible. Fish density (number of individuals per square kilometer; hereinafter, ind. km^{-2}) was estimated as the number of fish divided by the swept area. The mean body weight of each species was estimated as the total weight of the fish divided by the number of fish. We calculated the location of the center of the distribution of each species, weighted by the fish density as follows:

$$c_{\mathrm{lon}} = \frac{\sum_{i=1}^{n} \mathrm{lon}(i) \times fd(i)}{\sum_{i=1}^{n} fd(i)} \quad (6)$$

$$c_{\mathrm{lat}} = \frac{\sum_{i=1}^{n} \mathrm{lat}(i) \times fd(i)}{\sum_{i=1}^{n} fd(i)} \quad (7)$$

where c_{lon} and c_{lat} indicate the longitude and latitude of the center of the distribution, respectively, i indicates trawl observation, n indicates the number of trawl observations, $\mathrm{lon}(i)$ and $\mathrm{lat}(i)$ indicate longitude and latitude of trawl observation i, respectively, and $fd(i)$ indicates fish density of trawl observation i. The depth and bottom temperature at the center of the distribution were estimated from our 0.5′ latitude × 0.5′ longitude mesh bottom depth data and our gridded bottom temperature field in November during each year, respectively. The trends for the fish density, mean weight, c_{lon}, c_{lat}, and the depth and bottom temperature at the center of the distribution were calculated by linear regression using the least-squares method. The slopes of these trends were also

tested through a parametric test using Pearson's product-moment correlation coefficient.

3. RESULTS

3.1. Assessment of flexible Gaussian interpolation methods

To determine the optimal value for Z_0, we assessed the root-mean-square difference between T'_m and T_c using sensitivity analyses for Z_0 (Fig. 2a). Although the dependency of the root-mean-square difference on Z_0 was not clear, the root-mean-square difference was the lowest at Z_0 of 20 m (1.316°C). r^2 was 0.909 at Z_0 of 20 m and the highest among 6 cases (10–60 m in 10 m increments). From the results, we adopted 20 m for Z_0 to create the bottom temperature field. The bottom temperature field created had temperature distributions corresponding to the bathymetry (Fig. 2b, Fig. S2). In particular, steep temperature gradients along the continental slope at depths of 100–300 m were found. To estimate the optimum Z_0, T'_m excluding the temperature at the center of the interpolation circle (T_c) was calculated, as mentioned in Section 2. This value approximates the estimation error in a grid without including the bottom temperature measurement. To estimate an estimation error in a grid including a bottom temperature measurement, the root-mean-square differences and r^2 between the interpolated values (T'_m) including T_c and the observed value (T_c) were estimated. The root-mean-square differences and r^2 were 0.512°C and 0.984, respectively. In contrast, the bottom temperature field created using Eq. (1) exhibited a smoothed temperature distribution (Fig. 2c). The root-mean-square difference obtained from Eq. (1) was 2.452°C and was much larger than the differences obtained from Eq. (3) (Fig. 2a). The r^2 value obtained from Eq. (1) was 0.656. These results strongly suggest an improvement in the interpolation by including the effect of the difference in depth. Both the Gaussian interpolation weighting with distance (T_g) and the inverse distance interpolation (T_i) were low in interpolation performance (root-mean-square difference > 2.5°C and $r^2 < 0.60$).

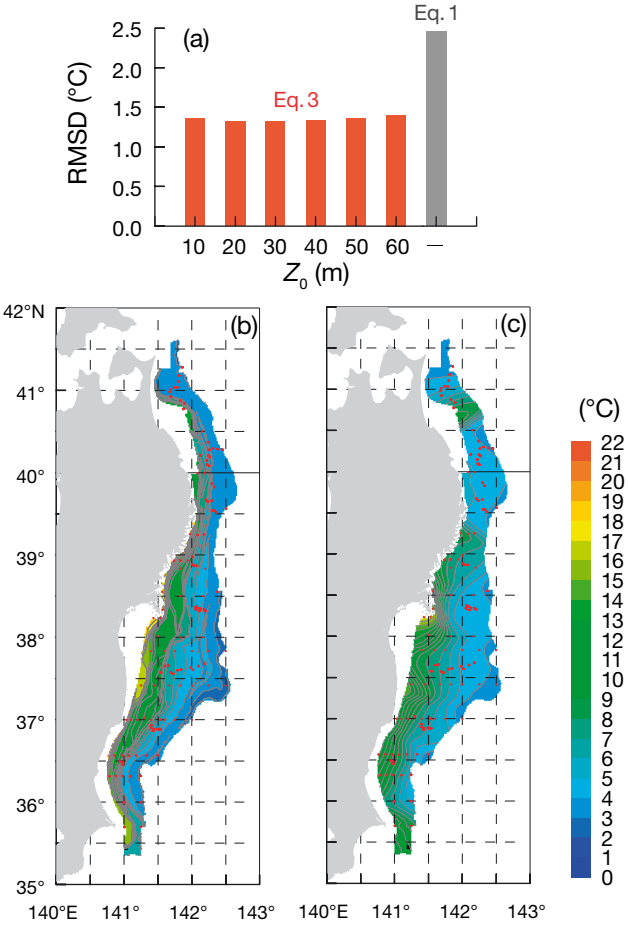

Fig. 2. (a) Root-mean-square difference between estimated temperature (T'_m) and observed temperature (T_c) based on sensitivity analyses for the interpolation scale for depth (Z_0), estimated from Eq. (1) (gray) and Eq. (3) (red). Z_0 is not included in Eq. (1). (b,c) Bottom temperature distributions during October 2018 obtained from (b) Eq. (3) and (c) Eq. (1). Red dots in (b,c): locations of the bottom temperature measurements. The color key indicates bottom temperature

3.2. Bottom temperature distribution

The monthly bottom temperature fields from 2003 to 2019, created using the Eq. (3), are shown in Fig. S2. The area where the bottom temperature is interpolated differs for each month. In April 2011, just after the earthquake and tsunami, the measurement was zero in the study area. Within 38°–38° 30′ N, 141°–141° 30′ E, i.e in Sendai Bay, there are always missing data areas because the bottom depth is lower than 50 m (Fig. 1b). Except for the missing data area, the bottom temperature was generally interpolated approximately 50–100 km off the coastline. The bottom temperature was high in shallower areas, and vice versa. The difference in the bottom temperature within depth zones was small, and isothermal lines were oriented in the north–south direction along the isobathymetric lines. However, there were seasonal and annual differences in the bottom temperatures, even within depth zones. For

example, the bottom temperatures in November 2007 and 2017 in the middle area were high (approximately 15°C within 50–100 m) and low (12 to 14°C within 50–100 m), respectively.

3.3. Spatially averaged bottom temperature in depth zones

Spatially averaged bottom temperature within the depth zones of 50–300 m with increments of 50 m in 3 regions (southern, middle and northern regions) was estimated from the gridded monthly bottom temperature field. The number of months for which the spatially averaged bottom temperature could not be estimated (due to missing data) in the southern, middle, and northern regions were 1–2, 2–5, and 11–17, respectively (Table 2). In April 2011, the average bottom temperatures were missing in all regions and depth zones, as mentioned in the previous paragraph. Except for April 2011, there were no missing data at 100–300 m in the southern region (there was 1 missing value for the depth zone of 50–100 m in August 2003).

Seasonal changes were observed in the bottom temperature (Fig. 3). The ranges of seasonal change were larger in the shallower zones, approximately 10 and 4°C within 50–100 m and 250–300 m, respectively. The maximum temperature in the 50–100 m depth zone was observed in October or November, while the maximum temperature in the 100–300 m depth zone was observed in November or December.

Table 2. Trend analysis for spatially averaged monthly bottom temperature in 5 depth zones in 3 regions. n: number of months for which the spatially averaged bottom temperature is available from 2003 to 2019; slope: slope of the trend; p: p-value obtained from a parametric test using Pearson's product-moment correlation coefficient

Region	Depth (m)	n	Slope (°C yr^{-1})	p
Northern	50–100	188	0.072	0.209
	100–150	192	0.053	0.176
	150–200	193	0.071	0.024
	200–250	188	0.089	0.008
	250–300	187	0.109	0.001
Middle	50–100	199	0.094	0.069
	100–150	202	0.072	0.057
	150–200	202	0.074	0.016
	200–250	202	0.063	0.012
	250–300	200	0.083	0.000
Southern	50–100	202	0.108	0.017
	100–150	203	0.088	0.012
	150–200	203	0.115	0.000
	200–250	203	0.103	0.000
	250–300	203	0.104	0.000

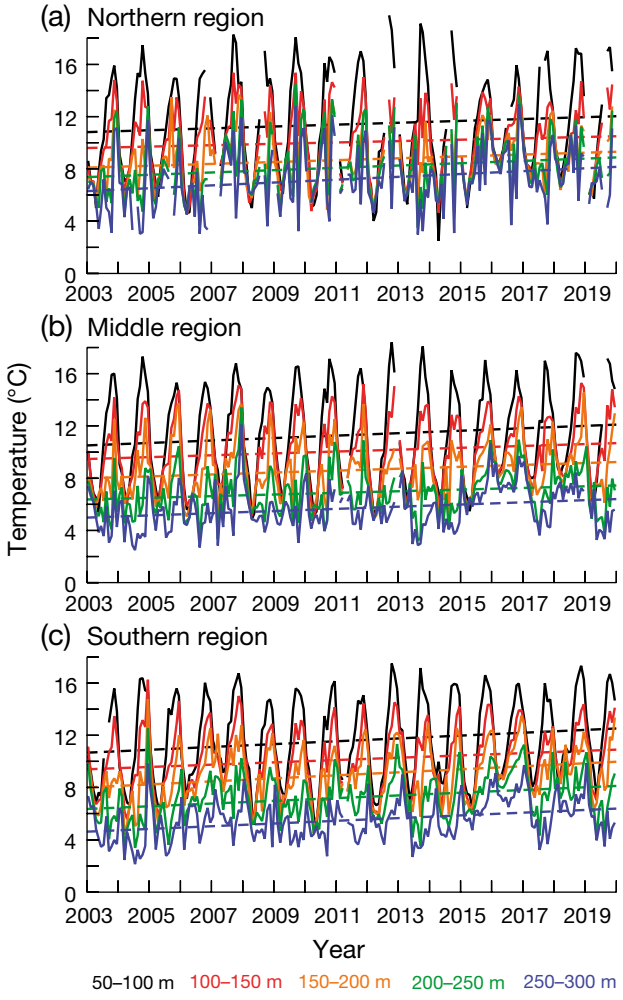

Fig. 3. Time series for spatially averaged monthly bottom temperature in 5 depth zones in 3 regions (a: northern, b: middle, and c: southern; see Fig. 1c for locations) (solid lines). Dashed lines: trend

Positive trends of 0.053 to 0.115°C yr^{-1} in the spatially averaged bottom temperature were found within all regions and all depth zones (Table 2). A significant positive trend ($p < 0.05$) was obtained in 11 areas (73%), and in 6 of them, a strong, significant warming trend ($p < 0.01$) was obtained. Stronger warming trends of 0.083 to 0.115°C yr^{-1} were found in deeper zones (150–300 m). The strongest warming trend (0.115°C yr^{-1}) was observed within a depth zone of 150–200 m in the southern region, and relatively high trends were also found in this region. Within a depth zone of 150–200 m in the southern region, the annual average temperature rose by 1.6°C during our study period (from 8.0°C in 2003 to 9.6°C in 2019).

To clarify the effect of adopting the deepest measurement within 30% of the bottom depth above the sea floor as the bottom temperature, we extracted the deepest measurement within 10% of the bottom depth above the sea floor. The number of adopted bottom temperatures in each month decreased to 65.0 ± 34.8. Owing to the decrease in available bottom temperature, the missing data area in the gridded monthly bottom temperature fields increased. Spatially averaged bottom temperatures within the depth zones of 50–300 m with increments of 50 m in the 3 regions had positive trends of 0.043 to 0.136°C yr^{-1} (Table S1). A significant positive trend ($p < 0.05$) was observed in 14 areas (93%), and 11 of them showed a strong, significant warming trend ($p < 0.01$). These results are approximately consistent with the original results; however, there were many months (73–99) for which the spatially averaged monthly bottom temperature was missing in the northern region.

3.4. Catch data of demersal fish in the middle region

Fig. 4 shows the catch data for 8 demersal fish landed in 9 fish markets in the middle region. The annual amount of landed Japanese flounder was 117–303 t from 2003 to 2012, increased to 1044–1698 t from 2013 to 2015, and slightly decreased to 726–1256 t after 2016 (Fig. 4a). Similar trends in the catch were found in ribbon fish (Fig. 4c), searobin (Fig. 4d), common octopus (Fig. 4e), and swimming crab (Fig. 4h), i.e. low catches occurred during the 2000s and the catches increased during the 2010s. In particular, for swimming crab, although there was no landing from 2003 to 2005 and the catches were a maximum of 8 t from 2006 to 2011, a landing of greater than 500 t was obtained from 2015 to 2018. An obvious increase in the catch of these species during summer (July–September) and autumn (October–December) was found to occur in recent years in this study. The catch of these species during winter (January–March) was generally lower than that during summer and autumn; however, it has also recently increased. The catch of the swimming crab during winter was 0 t prior to 2013, but was 1–32 t after 2014. A similar tendency was found in the catch of ribbon fish during winter and spring (April–June), i.e. 0–1 t prior to 2016 but 1–5 t after 2017. Spear squid were caught in large amounts after 2014; however, they were also occasionally caught before that year (e.g. 2007 and 2008) (Fig. 4g). The catch of Pacific cod was high (>8000 t) from 2004 to 2010 with large annual variations, but abruptly decreased to 3211 t in 2011

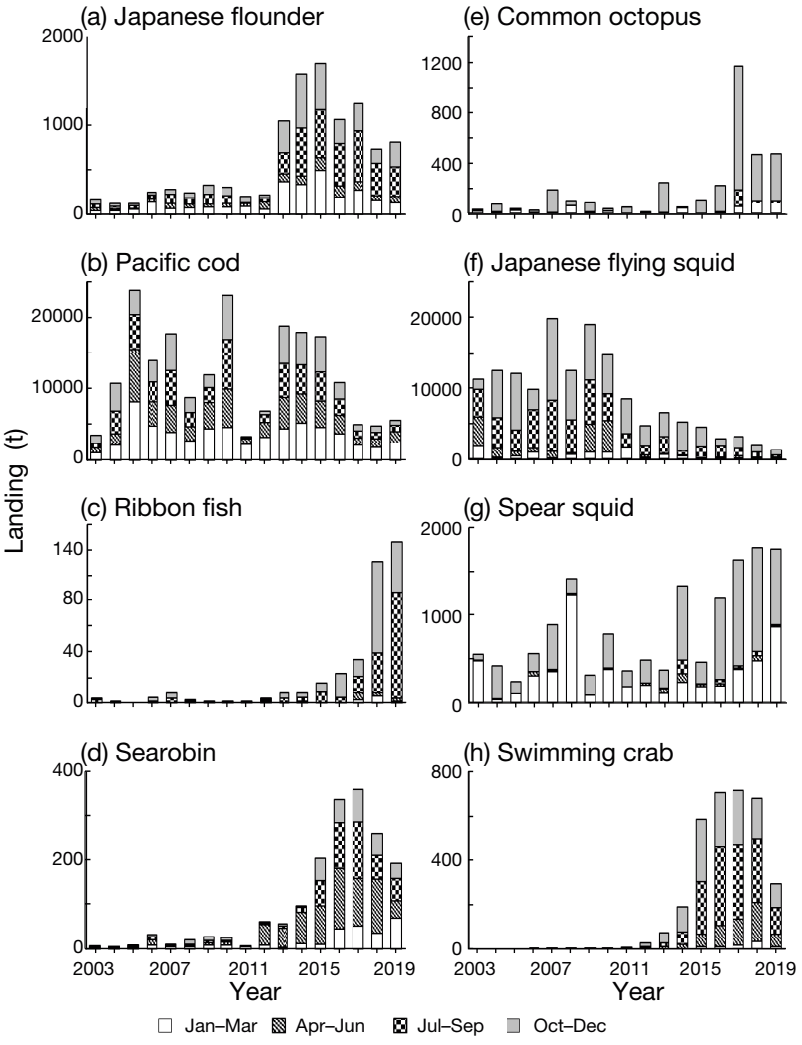

Fig. 4. Catch data for demersal fish from 2003 to 2019 in the middle region (see Fig. 1c): (a) Japanese flounder *Paralichthys olivaceus*, (b) Pacific cod *Gadus microcephalus*, (c) ribbon fish *Trichiurus lepturus*, (d) searobin *Lepidotrigla microptera*, (e) common octopus *Octopus sinensis*, (f) Japanese flying squid *Todarodes pacificus*, (g) spear squid *Heterololigo bleekeri*, and (h) swimming crab *Portunus trituberculatus*. For (c) and (h), we modified the graph reported by Okamura et al. (2021)

(Fig. 4b). Although it returned once to more than 10 000 t in 2013–2016, it remained at approximately 5000 t after 2017. A notable reduction in catch was found in Japanese flying squid; catch was more than 9000 t from 2003 to 2010 and gradually decreased to 1222 t in 2019 (Fig. 4f).

3.5. Distribution and density of non-target species in fisheries

The densities of blackbelly lantern shark obtained from bottom otter trawl surveys conducted during October–November are shown in Fig. S3. This species was mainly distributed in the southern and middle regions (36°–39° N) during the 2000s, but was distributed in all regions during the last half of the 2010s. The centers of the distribution of the species were mainly located at 36° 30′–37° N during the 2000s and moved northward to 38° 3′ N and 37° 47′ N in 2016 and 2018, respectively (Fig. 5a). The density of the species increased from 1025 ind. km^{-2} in 2003 to 12 827 ind. km^{-2} in 2019, and the trend was significantly positive ($p < 0.05$) (black line in Fig. 5b). The mean body weight of the fish gradually decreased from 0.16 kg in 2003 to 0.09 kg in 2019 with a significant trend ($p < 0.05$) (red line in Fig. 5b). The location (longitude and latitude) of the center of the distribution of the species showed a strong, significant positive trend ($p < 0.01$) (Fig. 5c). The depth at the center of the distribution of the species varied annually, ranging from

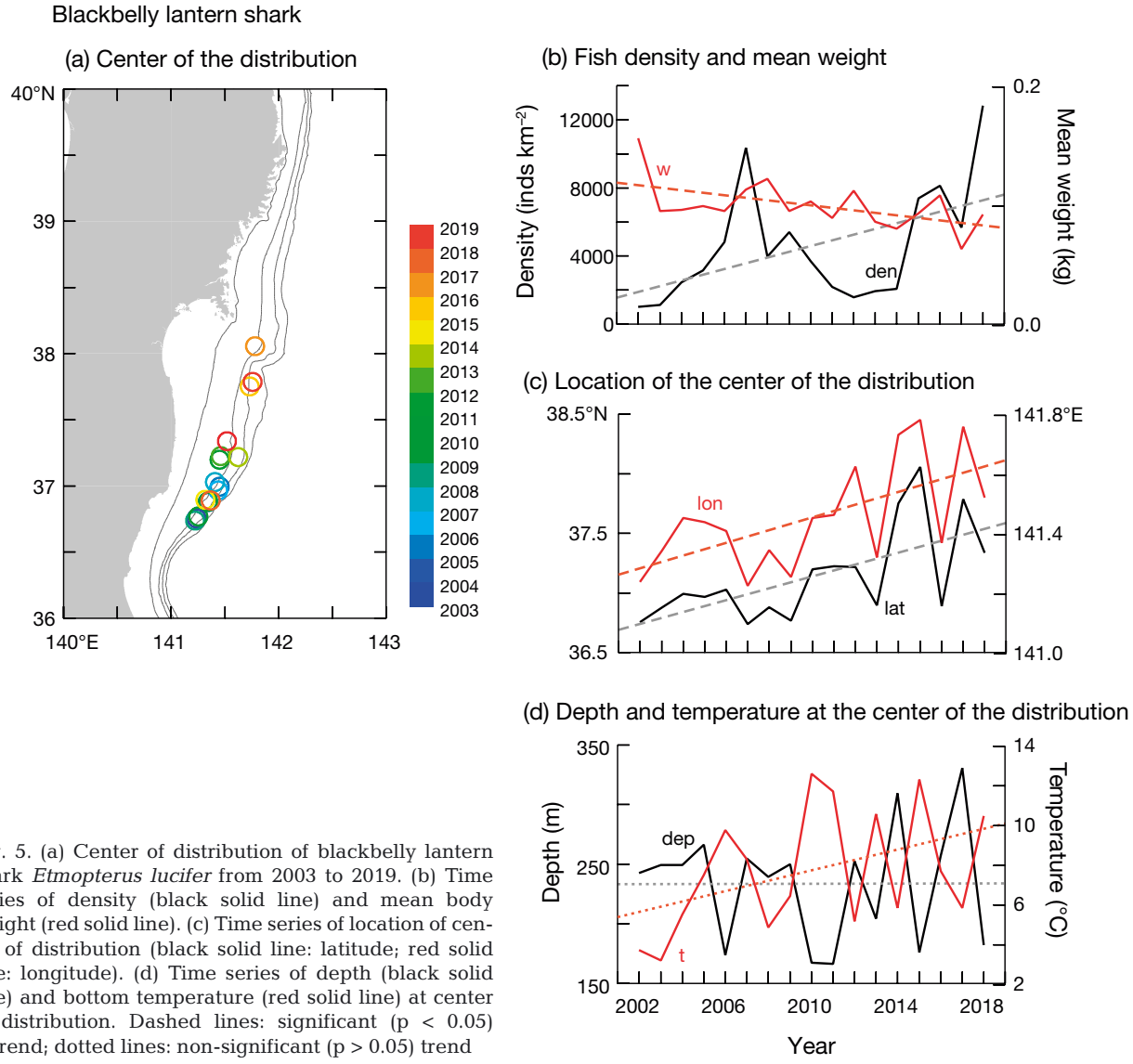

Fig. 5. (a) Center of distribution of blackbelly lantern shark *Etmopterus lucifer* from 2003 to 2019. (b) Time series of density (black solid line) and mean body weight (red solid line). (c) Time series of location of center of distribution (black solid line: latitude; red solid line: longitude). (d) Time series of depth (black solid line) and bottom temperature (red solid line) at center of distribution. Dashed lines: significant ($p < 0.05$) trend; dotted lines: non-significant ($p > 0.05$) trend

170 to 330 m, without a significant trend ($p > 0.05$) (black line in Fig. 5d). The bottom temperature at the center of the distribution of the species also did not show a significant trend ($p > 0.05$) (red line in Fig. 5d). These results indicate that this species shifted north-northeast without changes in the depth and temperature of its habitat.

The same distribution shift was found for bighand grenadier (Fig. S4, Fig. 6). The centers of the distribution of this species were mainly located at 36° 30′–37° N during the 2000s and moved northward to 38° 39′ N and 38° 11′ N in 2018 and 2019, respectively (Fig. 6a). The density of the species increased from 378 ind. km^{-2} in 2003 to 22 049 ind. km^{-2} in 2019, with a significantly positive trend ($p < 0.05$) (black line in Fig. 6b). The mean body weight of the fish varied annually, ranging from 0.19 to 0.36 kg, and the trend was not significant ($p > 0.05$) (red line in Fig. 6b). The trends in the location of the center of the distribution of the species showed a strong, significant positive trend ($p < 0.01$) (Fig. 6c). The depth at the center of the distribution of the species was approximately 150–300 m, except for 2004 (>400 m) (black line in Fig. 6d). The trends of the depth and bottom temperature at the center of the distribution were insignificant ($p > 0.05$) (Fig. 6d).

Deepsea bonefish (Fig. 7) also showed a significant positive trend in density ($p < 0.05$) (black line in Fig. 7b). The trend of the mean body weight of this fish was also significantly positive ($p < 0.05$) (red line in Fig. 7b). The latitude of the center of the distribution of this species was 36° 46′–38° 1′ N during our study period, and no significant trend was found (Fig. 7a,c, Fig. S5). The longitude moved

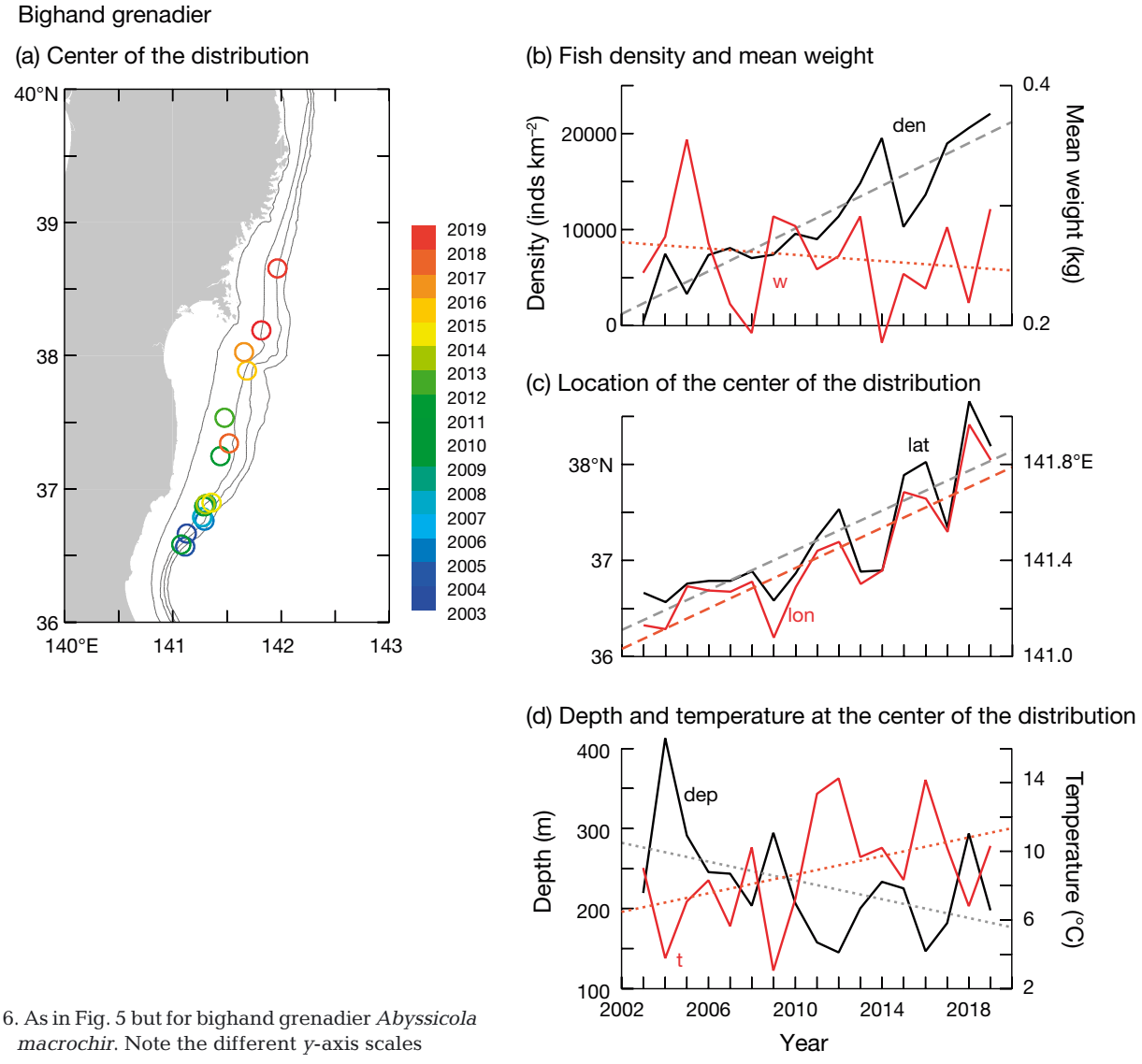

Fig. 6. As in Fig. 5 but for bighand grenadier *Abyssicola macrochir*. Note the different *y*-axis scales

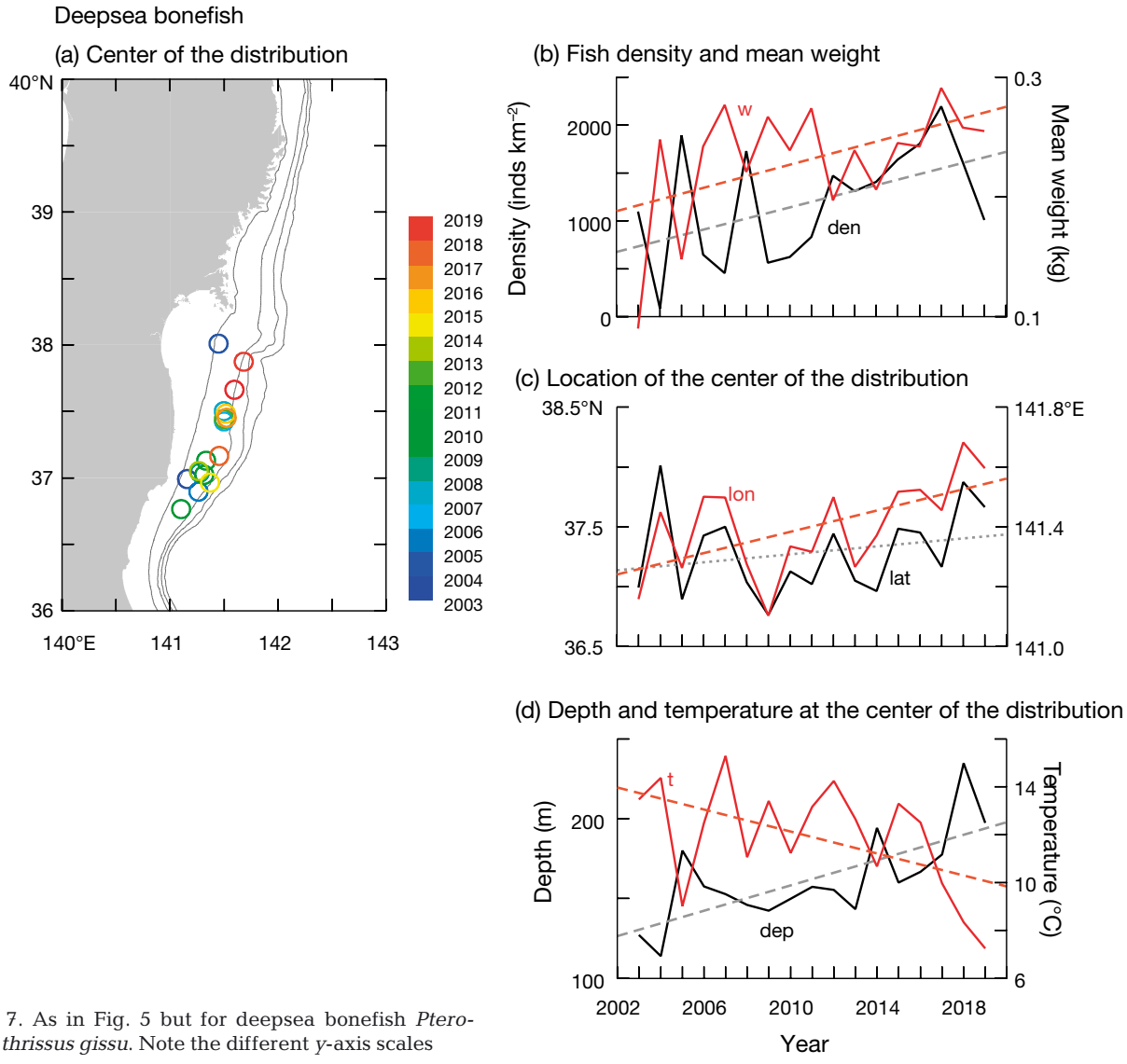

Fig. 7. As in Fig. 5 but for deepsea bonefish *Pterothrissus gissu*. Note the different *y*-axis scales

from 141° 9′ E in 2003 to 141° 41′ E in 2018, with a significant positive trend ($p < 0.05$). The depth at the center of the distribution of the species increased from approximately 120 m in 2003 and 2004 to approximately 200 m in 2018 and 2019 (black line in Fig. 7d). This trend was significantly positive ($p < 0.05$). The bottom temperature at the center of the distribution of the species showed a significant negative trend ($p < 0.05$) (red line in Fig. 7d). These results indicate that this species shifted to deeper waters, with an increase in density and mean body weight.

Darkfin sculpin and jelly eelpout exhibited the same tendencies as follows (Figs. S6 & S7 and Figs. 8 & 9). These species were widely distributed from the southern to northern regions during the 2000s with high density. In the following decade, however, they were less widely distributed and densities showed a significant downwards trend ($p < 0.01$). The locations of the center of distributions moved north-northeastward, with a significant trend ($p < 0.05$). The depth and bottom temperature at the center of the distributions did not show a significant trend ($p > 0.05$). These results indicate that these species shifted north-northeast without changes in the depth and temperature of their habitats, decreasing their densities. The only difference between these 2 species was that darkfin sculpin had a significant positive trend in mean body weight ($p < 0.05$), whereas there was no significant trend in the mean body weight of jelly eelpout ($p > 0.05$) (red line in Figs. 8b & 9b).

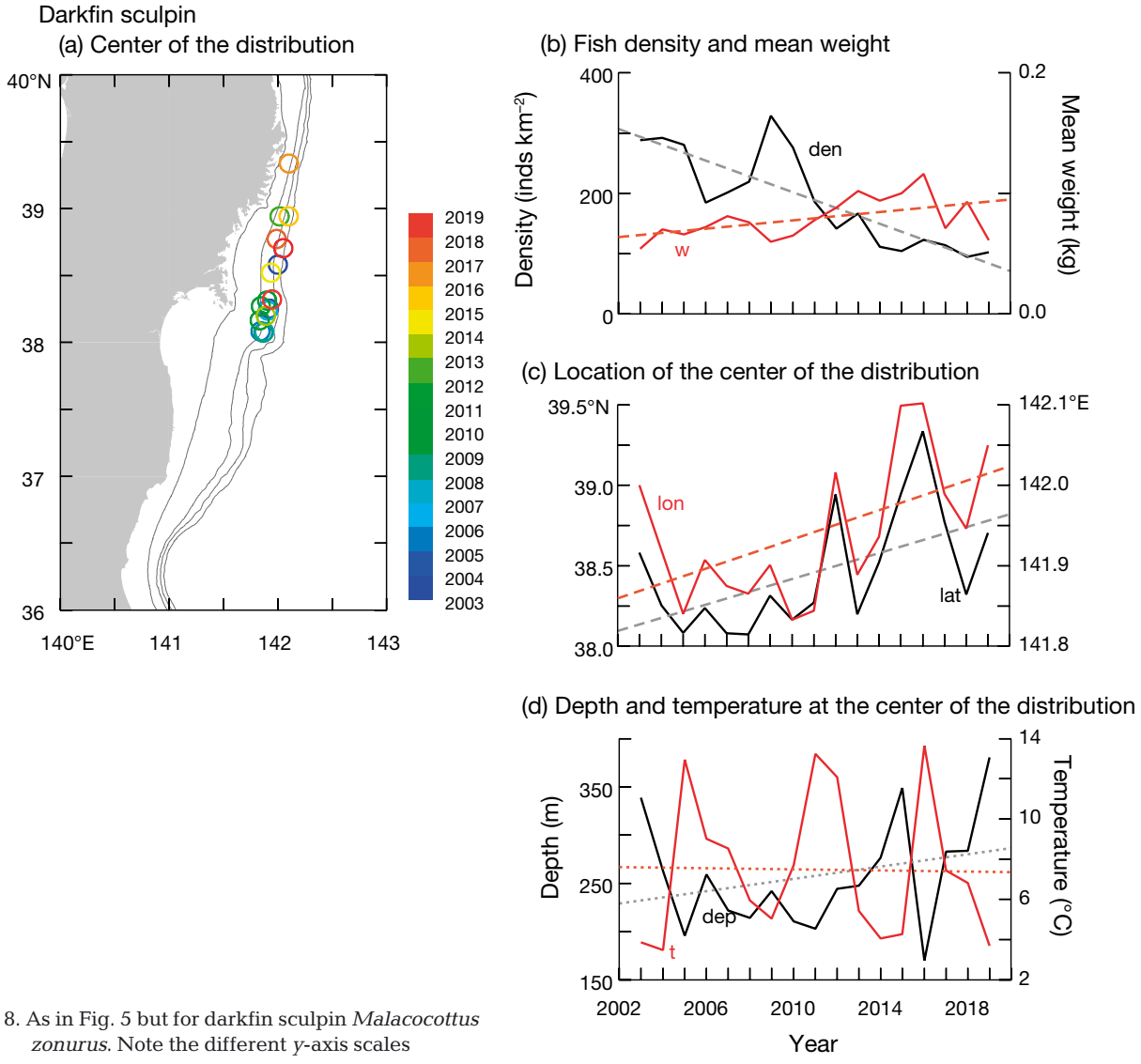

Fig. 8. As in Fig. 5 but for darkfin sculpin *Malacocottus zonurus*. Note the different *y*-axis scales

4. DISCUSSION

Our new extension of the Shimizu & Ito (1996) method, which accounts for depth differences, yielded the first bottom temperature distribution field estimates for the ocean off northeastern Japan. Accounting for the effect of depth at an interpolation scale of 20 m greatly improved the standard method. These results improve our understanding of the spatial and temporal variations in bottom temperature in the area, and they will be useful for validating the bottom temperature from an ocean circulation model.

However, there are some points that must be considered when using these bottom temperature fields. First, quality control of the extracted bottom temperatures was not conducted because of insufficient data; it is possible that some of the temperatures included were erroneous. When CTD data are registered to FRESCO, obvious erroneous temperatures such as <–3.0°C or >35.0°C are excluded by the system. Erroneous but not obviously wrong temperatures are more difficult to detect. Examining the obtained bottom temperature fields, we did not find any obvious erroneous temperature distributions, such as artificial local minimum and maximum temperatures. A method for detecting erroneous bottom temperatures by means of an objective analysis is needed, as Shimizu & Ito (1996) stated. Comparing the observed temperature to the climatological average (m) and standard deviation (σ) of temperature is one of the methods used to detect an erroneous value in observations. For example, when the difference

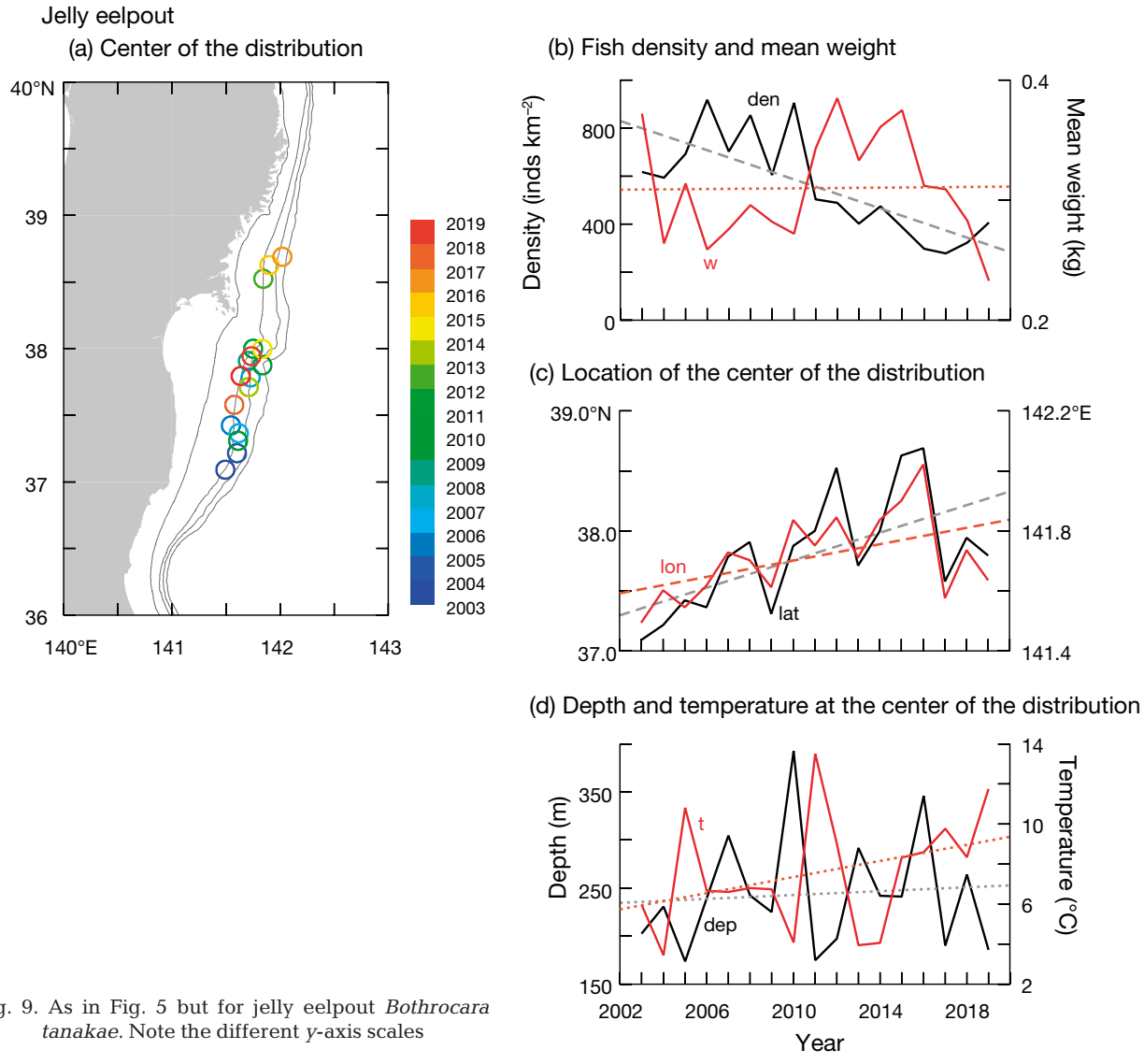

Fig. 9. As in Fig. 5 but for jelly eelpout *Bothrocara tanakae*. Note the different *y*-axis scales

between the observed temperature and m is greater than 4σ, the observed temperature is treated as erroneous data. Using our monthly bottom temperature fields from 2003 to 2019 constructed in this study, it is possible to create the climatological average and standard deviation of the bottom temperature for each month. The development of such a quality control method and incorporation into our bottom temperature interpolation method will be the subject of our future research.

The parameter values used in Eq. (3) must also be taken into consideration. Ito & Shimizu (1997) stated that approximately 5 d is desirable for the temporal interpolation scale (τ_0). However, because of insufficient data, we used 10 d for τ_0. Therefore, the estimated temperature is temporally smoothed. For Z_0, we adopted 20 m based on sensitivity analyses using other parameter values proposed by Shimizu & Ito (1996). Different optimal Z_0 values may be obtained from the analyses using different values of D_{min}, D_{max}, and τ_0.

While there are limitations as mentioned above, the bottom temperature fields obtained allowed us to clarify the interannual changes in bottom temperature in the area. Strong, significant warming trends ($p < 0.01$) of 0.083 to 0.115°C yr^{-1} were found in 40% (6 areas) of all regions and depth zones (Table 2), indicating bottom temperature warming. These trends were observed in the deeper zones (150–300 m). A strong significant positive trend of 0.76°C per 100 yr ($p < 0.01$) was detected in the sea surface temperature by the Japan Meteorological Agency, as mentioned in

Section 1. In the shallower depth zones in our study (50–100 m), the positive bottom temperature trend was generally not significant ($p > 0.05$, Table 2). This may be due to the differences in the analysis period; the data duration of the Japan Meteorological Agency is approximately 110 yr, whereas our data duration is 17 yr. Additionally, the rate of increase in bottom temperature obtained in our study was approximately 10 times that of the sea surface reported by the Japan Meteorological Agency. Because our study period was relatively short (17 yr), it may have been affected by factors other than long-term climate change.

One possible driver of change to water temperature in the western North Pacific is the Pacific Decadal Oscillation (PDO) (Mantua et al. 1997). Sea surface temperature around the western North Pacific is negatively correlated with the PDO (Mantua et al. 1997). The PDO index (https://psl.noaa.gov/pdo/, last accessed 20 May 2021) during our study period was as follows: positive values were observed from 2003 to 2005 and from 2014 to 2017, and negative values were observed during the remaining years. Because this annual variation of PDO does not synchronize with our spatially averaged monthly bottom temperature, it is considered that there is almost no effect of PDO on the bottom temperature increase in our study area. The North Pacific Gyre Oscillation (NPGO) (Di Lorenzo et al. 2010), with which the sea surface temperature around the western North Pacific has a negative correlation, decreased from positive values in the 2000s to negative values in the 2010s (www.o3d.org/npgo/, last accessed 20 May 2021). This coincided with an increasing temperature trend in our study area; therefore, our detected increase in bottom temperature may be influenced by the NPGO. Kutsuwada et al. (2008) reported that a rapid decrease in temperature occurred during the first half of the 1980s in the offshore area of our northern region (39° 15′ N, 143° 3′ E), and the temperature remained low until the 2000s. Because our analysis period starts during this low-temperature period, a subsequent temperature increase may lead to this high rate of temperature increase. Similar or higher rates of increasing trends in bottom temperature have been reported in previous studies, such as 1.6°C over 25 yr (=0.064°C yr^{-1}) in the North Sea (Dulvy et al. 2008) and 0.19°C yr^{-1} on the Scotian Shelf of eastern Canada (Brickman et al. 2018), supporting our results in this study.

Our study revealed the impact on demersal fish of a rapid increase in the bottom temperature. From the analysis of the catch data within the middle region, recent increases in the catches of warm-water species (Japanese flounder, ribbon fish, searobin, common octopus, spear squid, and swimming crab) were found (Fig. 4). For Japanese flounder, Kurita et al. (2018) reported that the stock level of the species off northeastern Japan remained high after 2013 because a dominant year-class occurred in 2010 and fishery operations decreased owing to the earthquake, tsunami, and the FDNPP accident. Therefore, factors other than bottom temperature warming affected the increase in the catch of this species. In the Southern Brazil Subtropical Convergence ecosystem, ribbon fish began to be caught at bottom temperatures of greater than 11°C (Martins & Haimovici 1997). Our study shows that there were 5 or 6 months in which bottom temperatures were greater than 11°C within 50–100 m of the middle region before 2014; this increased to 6 or 7 months after 2015. This increase in duration when the optimum temperature is distributed is considered to lead to an increase in the catch of the fish. Searobin in Mutsu Bay are widely distributed throughout the bay during summer, but are limited to warm areas (6 to 9°C) during winter (Fujioka et al. 1990). The increase in catch is considered to be influenced by bottom temperature warming within the middle region. The catch of common octopus in the middle region depends on the northward transport of juvenile octopus from the southern region, and recruitment is prevented by cold water masses that are distributed within the middle region (Akimoto & Sato 1980). Owing to bottom temperature warming within the middle region, the successful recruitment is considered to have resulted in an increase in catch. The catch per unit effort of spear squid within the middle region has a positive relationship with temperature (Tian et al. 2013), supporting the argument that the increase in the catch of the species is affected by bottom temperature warming. The distribution area and fishery grounds of swimming crab are mainly shallower than 50 m in depth. Although our bottom temperature analysis does not cover their main distribution area, increases in temperature within the depth zone of 50–100 m, adjacent to the area, and at the sea surface (Japan Meteorological Agency) were observed. The catch of crab is also considered to be affected by temperature warming. Ribbon fish and swimming crab were not caught during winter in the 2000s and the early 2010s, but began to be caught during winter in recent years (Fig. 4c,h), suggesting that they have been able to overwinter within the middle region of our study area and may have been reproducing within this region. This speculation is supported by Yagura (2021), who reported that

ovigerous females and juvenile crabs were caught from the middle region. For ribbon fish, many small individuals have been caught in recent years (approximately after 2017) by bottom otter trawl surveys conducted in the middle region of our study area in December from 2014 to 2020 by the R/V 'Wakataka-maru', supporting our speculation.

Some species had increased catches, whereas others had decreased catches. The catch of Japanese flying squid decreased from more than 9000 t before 2010 to 1222 t in 2019 (Fig. 4f). Their catch in Japan showed a decreasing trend after 1996 (Fisheries Agency of Japan and Japan Fisheries Research and Education Agency 2020a). The decrease in the catch of this species in our middle region is considered to be influenced by a decrease in the whole stock size of the species. The catch of Pacific cod, cold-water species, decreased after 2017, despite large annual variations (Fig. 4b). The stock level of the fish in northeastern Japan remained high from 2011 to 2015 owing to the decreased fishery operations; however, it decreased after 2016 (Fisheries Agency of Japan and Japan Fisheries Research and Education Agency 2020b). The decrease in the catch of the species within the middle region is supposed to correspond to these stock-level changes. Narimatsu et al. (2017) analyzed the same bottom trawl data we used and reported that the abundance of Pacific cod decreased after 2015. The recent decrease in stock level may be due to a warming of the bottom temperature. As for target fish in commercial fisheries, Shibata et al. (2021) also analyzed the same trawl data we used and reported that catch of snow crab *Chionoecetes opilio* significantly deceased after 2011. Because the crab is a cold-water species, it is thought that a warming of the bottom temperature in the study area has a strong influence on the species.

The impact of bottom water warming on non-target demersal fish in the fisheries was also examined (Section 3.5). The 5 analyzed non-target demersal fish in the fisheries were mainly distributed within the 150–300 m depth zone, where strong, significant warming trends of 0.083 to 0.115°C yr^{-1} were observed at the spatially averaged bottom temperature (Table 2). A distribution shift and change in density were found, indicating that they are strongly affected by bottom temperature warming. The patterns of distribution shift and density change differed for each species. This suggests that their sensitivity to warming varies on a species-specific basis.

Blackbelly lantern shark, which is found in temperate waters (40° N to 48° S) (Galland 2015), shifted north-northeastward with increasing density from 2003 to 2019 (Fig. 5). Because significant trends were not found for either the depth or bottom temperature at the center of the distribution, the species is supposed to have shifted northward along a suitable depth zone with the northward movement of the suitable bottom temperature zone owing to bottom temperature warming. Their northward shift along the suitable depth zone resulted in a north-northeastward shift of the center of distribution, because isobathymetric lines around their habitat are mainly oriented in the north-northeast–south-southwest direction. Because the species' densities have increased, bottom temperature warming appears to have led to the success of their survival and recruitment. The mean body weight of the species gradually decreased with a significant trend ($p < 0.05$) (black line in Fig. 5b). This may have occurred as a result of the northward shift of the reproductive grounds and the increase in small individuals with low migratory capacity within the area.

Bighand grenadier, the predominant species at depths of 300–500 m in the southern region of our study area (Fujiwara et al. 2005, Hattori et al. 2008), was also thought to have shifted northward along a suitable depth zone with the northward movement of the suitable bottom temperature zone. Bottom temperature warming would also lead to the success of their survival and recruitment.

The density and mean body weight of deepsea bonefish also increased during the 2010s; however, no significant trend was found in the latitude of their center of distribution. Instead, they shifted to deeper waters with a decrease in habitat temperature (Fig. 7d). To avoid warmer temperatures, species can shift to higher latitudes or deeper waters without a change in habitat temperature. Deepsea bonefish shifted deeper into colder waters. Because the mean body weight of the fish increased significantly ($p < 0.05$), the shift may be a bigger–deeper phenomenon (Polloni et al. 1979, Stefanescu et al. 1992). There is another possibility for the mechanism of the shift. According to Aguzzi et al. (2018), deepsea bonefish are dominant within the 500 m depth zone in Sagami Bay. This suggests that the distribution depth in our study area during the 2000s (approximately 120 m) was much shallower than their suitable depth zone. We believe that during the 2000s there was a reason (possibly competition from other species) why they remained in shallower waters than their preferred range.

Darkfin sculpin and jelly eelpout shifted northward, decreasing their density from the 2000s to 2010s (Figs. 8 & 9). The former and the latter are mainly dis-

tributed within the northern part of the North Pacific (Stevenson 2015, Glubokov et al. 2019) and northern Japan (Anderson et al. 2009), respectively, indicating that they are cold-water fish. We consider that they shifted their distribution northward owing to bottom water warming. The observation that there was a significant positive trend in the mean body weight of darkfin sculpin, despite their decreased density, suggests that the success of recruitment may have recently decreased, resulting in an increase in the proportion of aged fish over young fish.

Thus, we have clarified the distribution shifts and density changes in 5 demersal fishes. These changes differed among species. These fishes, except for deepsea bonefish, did not show significant changes in habitat temperature or depth. The insignificant change in depth could be explained by pressure adaptation limitations (Brown & Thatje 2014). Perry et al. (2005) stated that almost half of the examined demersal species shifted northward as a result of warming in the North Sea. In the Bay of Biscay, a shift towards deeper areas was the dominant movement (28%) for demersal fish studied (Punzón et al. 2016). Thus, the responses of demersal fish to temperature warming also differ among sea areas. Regarding climate-driven distribution shifts, Burrows et al. (2014) concluded that climate velocity, which can be described as the speed and direction of isotherms, is emerging as a good predictor of range shifts in the ocean. We expect an analysis related to climate velocity in our study area using our monthly mean temperature fields to be conducted in future studies.

The results relating to non-target demersal fish in the fisheries were obtained from the trawl survey data conducted from October to November. Because the bottom temperature changes seasonally, the distribution of these species may also shift seasonally. This issue will be addressed in a future study. Another point we should pay attention to is the oxygen minimum zone, which possibly influences the composition and diversity of demersal fish communities (Gallo & Levin 2016). The oxygen minimum zone is located at depths of 600–1000 m in our study area, and the dissolved oxygen concentration in the zone is approximately 50 µmol l^{-1}, based on Keeling et al. (2010). Therefore, the distribution of the oxygen minimum zone affects the habitats of the target species in our bottom otter trawl surveys. In the Gulf of California, the temperature best explains the variance in density of deep-sea fishes, whereas oxygen best explains the variance in their diversity and community composition (Gallo et al. 2020). Demersal fisheries are likely to be negatively impacted by the expansion of the oxygen minimum zone in a warming ocean (Gallo & Levin 2016). Interannual and seasonal variations in bottom oxygen concentration should also be considered in future studies. Creating a bottom oxygen field using our interpolation method will be useful if adequate bottom oxygen data are made available. The impact of bottom temperature warming combined with deoxygenation on other demersal fishes should also be examined in a future study.

5. CONCLUSIONS

We have developed a new method for creating bottom temperature field data using a flexible Gaussian filter weighting with time, distance, and depth. Bottom temperature fields from 2003 to 2019 off the Pacific coast of northeastern Japan were created using this method. Spatially averaged bottom temperature had a strong, significant warming trend of 0.083 to 0.115°C yr^{-1} within depth zones of 150–300 m, thus providing evidence of bottom water warming in this area. Corresponding to such warming, increases in landing amounts were found for warm-water species such as ribbon fish, searobin, common octopus, and swimming crab in fish markets located within the middle region (37° 50′–39° N). This is an indication that ribbon fish and swimming crab may recently have been overwintering and reproducing in the region. For non-target species in fisheries, distribution shifts and changes in density were observed from 2003 to 2019. Blackbelly lantern shark and bighand grenadier shifted northward, increasing their density, indicating that bottom temperature warming led to an expansion of their habitat. Conversely, darkfin sculpin and jelly eelpout shifted northward, decreasing in density, suggesting that bottom temperature warming had a negative effect on them in the study region. Deepsea bonefish shifted into deeper and colder waters with increasing density. Factors other than bottom temperature warming may have contributed to this shift. Thus, changes that are considered to be induced by bottom temperature warming have been revealed. As responses differ among species, it will be important in future studies to examine the effects of bottom temperature warming on each specific species.

Data availability. The temperature data used in this study are available from FRESCO (https://www.fresco.jafic.or.jp/, last accessed 9 Mar 2021). However, this site can be accessed only by members. The fishery data that support the findings of this study are available from the corresponding author upon reasonable request.

Acknowledgements. We thank R. Misawa of the Japan Fisheries Research and Education Agency for the useful comments. This research was supported by the following projects: the Reconstruction Program funded by the Japan Fisheries Research and Education Agency; Stock Assessment Program funded by the Japan Fisheries Research and Education Agency of Japan and Fisheries Agency; A Scheme to Revitalize Agriculture and Fisheries in a Disaster Area through Deploying Highly Advanced Technology, funded by the Agriculture, Forestry, and Fisheries Research Council and Reconstruction Agency, Japan; and the Environment Research and Technology Development Fund (JPMEERF20S11809) of the Environmental Restoration and Conservation Agency of Japan. We thank Editage English Editing Services for editing the draft of this manuscript. We thank the 3 anonymous reviewers for their constructive comments and the editor for reviewing the manuscript.

LITERATURE CITED

Aguzzi J, Fanelli E, Ciuffardi T, Schirone A and others (2018) Faunal activity rhythms influencing early community succession of an implanted whale carcass offshore Sagami Bay, Japan. Sci Rep 8:11163

Akimoto Y, Sato T (1980) Regional foundation studies on the ecology of *Octopus vulgaris* LAMARCK-I. On the fluctuation of catches and migration. Bull Fukushima Prefect Fish Exp Stn 6:11–19 (in Japanese)

Anderson ME, Stevenson DE, Shinohara G (2009) Systematic review of the genus *Bothrocara* Bean 1890 (Teleostei: Zoarcidae). Ichthyol Res 56:172–194

Brickman D, Hebert D, Wang Z (2018) Mechanism for the recent ocean warming events on the Scotian Shelf of eastern Canada. Cont Shelf Res 156:11–22

Brown A, Thatje S (2014) Explaining bathymetric diversity patterns in marine benthic invertebrates and demersal fishes: physiological contributions to adaptation of life at depth. Biol Rev Camb Philos Soc 89:406–426

Burrows MT, Schoeman DS, Richardson AJ, Molinos JG and others (2014) Geographical limits to species-range shifts are suggested by climate velocity. Nature 507:492–495

Cheung WW, Watson R, Pauly D (2013) Signature of ocean warming in global fisheries catch. Nature 497:365–368

Di Lorenzo E, Cobb KM, Furtado JC, Schneider N and others (2010) Central Pacific El Niño and decadal climate change in the North Pacific Ocean. Nat Geosci 3: 762–765

Doney SC, Ruckelshaus M, Duffy JE, Barry JP and others (2012) Climate change impacts on marine ecosystems. Annu Rev Mar Sci 4:11–37

Dulvy NK, Rogers SI, Jennings S, Stelzenmuller V, Dye SR, Skjoldal HR (2008) Climate change and deepening of the North Sea fish assemblage: a biotic indicator of warming seas. J Appl Ecol 45:1029–1039

Ebert DA, Fowler SL, Compagno LJ, Dando M (2013) Sharks of the world: a fully illustrated guide. Wild Nature Press, Plymouth, p 528

Endo Y (2000) Management of krill fisheries in Japanese waters. In: Everson I (ed) Krill: biology, ecology and fisheries. Blackwell Science, Oxford, p 284–299

Fisheries Agency of Japan and Japan Fisheries Research and Education Agency (2020a) Stock assessment and resource evaluation for Japanese common squid in autumn group (fiscal year 2019). http://abchan.fra.go.jp/digests2019/details/201919.pdf (in Japanese) (last accessed 9 Mar 2021)

Fisheries Agency of Japan and Japan Fisheries Research and Education Agency (2020b) Stock assessment and resource evaluation for Pacific cod in the Pacific coast of northern Japan (fiscal year 2019). http://abchan.fra.go.jp/digests2019/details/201930.pdf (in Japanese) (last accessed 9 Mar 2021)

Free CM, Thorson JT, Pinsky ML, Oken KL, Wiedenmann J, Jensen OP (2019) Impacts of historical warming on marine fisheries production. Science 363:979–983

Fujioka T, Takahasi T, Maeda T, Nakatani T, Matsushima H (1990) Annual life cycle and distribution of adult gurnard *Lepidotrigla microptera* in Mutsu Bay, Aomori Prefecture. Bull Jpn Soc Sci Fish 56:1553–1560 (in Japanese with English Abstract)

Fujita T, Inada T, Ishito Y (1993) Density, biomass and community structure of demersal fishes off the Pacific coast of northeastern Japan. J Oceanogr 49:211–229

Fujita T, Inada T, Ishito Y (1995) Depth-gradient structure of the demersal fish community on the continental shelf and upper slope off Sendai Bay, Japan. Mar Ecol Prog Ser 118:13–23

Fujiwara K, Katayama S, Omori M, Kitagawa D (2005) Seasonal distribution of *Abyssicola macrochir* (Guenter) on the upper continental slope off the southern Tohoku coast, northeastern Japan, in relation to their life history. Bull Jpn Soc Fish Oceanogr 69:83–90

Galland AR (2015) Demographics of *Etmopterus lucifer* (lucifer dogfish). MSc thesis, Victoria University of Wellington

Gallo ND, Levin LA (2016) Fish ecology and evolution in the world's oxygen minimum zones and implications of ocean deoxygenation. Adv Mar Biol 74:117–198

Gallo ND, Beckwith M, Wei CL, Levin LA, Kuhnz L, Barry JP (2020) Dissolved oxygen and temperature best predict deep-sea fish community structure in the Gulf of California with climate change implications. Mar Ecol Prog Ser 637:159–180

Glubokov AI, Glubokovskii MK, Kovacheva NP (2019) New data on soft sculpin *Malacocottus zonurus* (Psychrolutidae) from the northwestern Bering Sea. J Ichthyol 59: 435–438

Hanawa K, Mitsudera H (1986) Variation of water system distribution in the Sanriku coastal area. J Oceanogr Soc Jpn 42:435–446

Hattori T, Narimatsu Y, Ito M, Ueda Y, Kitagawa D (2008) Annual changes in distribution depths of bighand thornyhead *Sebastolobus macrochir* off the Pacific coast of northern Honshu, Japan. Fish Sci 74:594–602

Hattori T, Okuda T, Narimatsu Y, Ito M (2010) Distribution patterns of five pleuronectid species on the continental slope off the Pacific coast of northern Honshu, Japan. Fish Sci 76:747–754

Hoegh-Guldberg O, Bruno JF (2010) The impact of climate change on the world's marine ecosystems. Science 328: 1523–1528

IPCC (Intergovernmental Panel on Climate Change) (2014) Core Writing Team, Pachauri RK, Meyer LA (eds) Climate change 2014: synthesis report. Contribution of Working Groups I, II and III to the Fifth Assessment Report of the Intergovernmental Panel on Climate Change. IPCC, Geneva

Ito S (2001) Physical and lower-trophic level data time-series in the Mixed Water Region. In: Alexander V, Bychkov

AS, Livingston P, McKinnell SM (eds) Impact of climate variability on observation and prediction of ecosystem and biodiversity changes in the North Pacific. PICES Sci Rep 18. North Pacific Marine Science Organization (PICES), Sidney, BC, p 107–111

Ito S, Shimizu Y (1997) Distribution patterns of temperature data and a method to draw isotherms in the Tohoku offshore area. Bull Tohoku Natl Fish Res Inst 59:163–170 (in Japanese with English Abstract)

Jereb P, Roper CFE (2010) *Heterololigo bleekeri*. In: Jereb P, Roper CFE (eds) Cephalopods of the world, Vol 2, myopsid and oegopsid squids. Food and Agriculture Organization of the United Nations (FAO), Rome, p 71–72

Katayama S, Ishida T, Shimizu Y, Yamanobe A (2004) Seasonal change in distribution of Conger eel *Conger myriaster* off the Pacific coast south of Tohoku, north-eastern Japan. Fish Sci 70:1–6

Kawabata A, Yatsu A, Ueno Y, Suyama S, Kurita Y (2006) Spatial distribution of the Japanese common squid, *Todarodes pacificus*, during its northward migration in the western North Pacific Ocean. Fish Oceanogr 15:113–124

Kawai H (1972) Hydrography of the Kuroshio Extension. In: Stommel H, Yoshida K (eds) Kuroshio: its physical aspects. University of Tokyo Press, Tokyo, p 235–352

Keeling RF, Kortzinger A, Gruber N (2010) Ocean deoxygenation in a warming world. Annu Rev Mar Sci 2: 199–229

King NJ, Bagley PM, Priede IG (2006) Depth zonation and latitudinal distribution of deep-sea scavenging demersal fishes of the Mid-Atlantic Ridge, 42 to 53° N. Mar Ecol Prog Ser 319:263–274

Kurita Y, Togashi H, Hattori T, Shibata Y (2018) Stock assessment and resource evaluation for Japanese flounder in the Pacific coast of northern Japan (fiscal year 2017). Marine fisheries stock assessment and evaluation of Japanese waters 1672–1700 (in Japanese). http://abchan.fra.go.jp/digests2017/details/201757.pdf

Kuroda H, Setou T, Kakehi S, Ito S and others (2017) Recent advances in Japanese fisheries science in the Kuroshio-Oyashio region through development of the FRA-ROMS Ocean Forecast System: overview of the reproducibility of reanalysis products. Open J Mar Sci 7:62–91

Kutsuwada K, Hattori M, Yamada Y (2008) Long-term variability of upper oceanic condition off the Sanriku Coast. Oceanogr Jpn 17:19–38 (in Japanese with English Abstract)

Mantua NJ, Hare SR, Zhang Y, Wallace JM, Francis RC (1997) A Pacific interdecadal climate oscillation with impacts on salmon production. Bull Am Meteorol Soc 78: 1069–1080

Martins AS, Haimovici M (1997) Distribution, abundance and biological interactions of the cutlassfish *Trichiurus lepturus* in the southern Brazil Subtropical Convergence ecosystem. Fish Res 30:217–227

Menezes GM, Sigler MF, Silva HM, Pinho MR (2006) Structure and zonation of demersal fish assemblages off the Azores Archipelago (mid-Atlantic). Mar Ecol Prog Ser 324:241–260

Ministry of Agriculture, Forestry and Fisheries (2021) Fisheries and aquaculture statistics in 2019. https://www.e-stat.go.jp/stat-search/filedownload?statInfId=000032044765&fileKind=0 (last accessed 9 Mar 2021)

Mishima S (1984) Stock assessment and biological aspects of Pacific cod (*Gadus macrocephalus* Tilesius) in Japanese waters. INPFC Bull 42:180–199

Miyake S (ed) (1991) Blue swimming crab. In: Japanese crustacean decapods and stomatopods in color (Vol II). Hoikusha, Osaka, p 277

Nakabo T, Doiuchi R (2013a) Paralichthyidae. In: Nakabo T (ed) Fishes of Japan with pictorial keys to the species, 3rd edn. Tokai University Press, Hadano, p 1659–1661 (in Japanese)

Nakabo T, Doiuchi R (2013b) Trichiuridae. In: Nakabo T (ed) Fishes of Japan with pictorial keys to the species, 3rd edn. Tokai University Press, Hadano, p 1644–1647 (in Japanese)

Narimatsu Y, Sohtome T, Yamada M, Shigenobu Y, Kurita Y, Hattori T, Inagawa R (2015) Why do the radionuclide concentrations of Pacific cod depend on the body size? In: Nakata K, Sugisaki H (eds) Impact of the Fukushima nuclear accident on fish and fishing grounds. Springer Japan, Tokyo, p 123–138

Narimatsu Y, Shibata Y, Hattori T, Yano T, Nagao J (2017) Effects of a marine-protected area occurred incidentally after the Great East Japan Earthquake on the Pacific cod (*Gadus macrocephalus*) population off northeastern Honshu, Japan. Fish Oceanogr 26:181–192

Norman MD, Hochberg FG, Finn JK (2014) *Octopus vulgaris*. In: Jereb P, Roper CFE, Norman MD, Finn JK (eds) Cephalopods of the world, Vol 3. Octopods and vampire squids. Food and Agriculture Organization of the United Nations (FAO), Rome, p 42–47

Okamura Y, Masuda Y, Yagura A, Tanabe T, Abe N, Gambe S (2021) Recent changes in fisheries catch compositions and oceanic conditions off Miyagi prefecture. Fish Biol Oceanogr Kuroshio 22:41–46 (in Japanese)

Perry AL, Low PJ, Ellis JR, Reynolds JD (2005) Climate change and distribution shifts in marine fishes. Science 308:1912–1915

Polloni PT, Haedrich RL, Rowe GT, Clifford CH (1979) The size–depth relationship in deep ocean animals. Int Rev Gesamten Hydrobiol Hydrogr 64:39–46

Punzón A, Serrano A, Sanchez F, Velasco F, Preciado I, Gonzalez-Irusta JM, Lopez-Lopez L (2016) Response of a temperate demersal fish community to global warming. J Mar Syst 161:1–10

Sedberry GR, Van Dolah RF (1984) Demersal fish assemblages associated with hard bottom habitat in the South Atlantic Bight of the USA. Environ Biol Fishes 11: 241–258

Shibata Y, Sakuma T, Wada T, Kurita Y and others (2017) Effect of decreased fishing effort off Fukushima on abundance of Japanese flounder (*Paralichthys olivaceus*) using an age-structured population model incorporating seasonal coastal-offshore migrations. Fish Oceanogr 26: 193–207

Shibata Y, Nagao J, Narimatsu Y, Morikawa E and others (2021) Estimating the maximum sustainable yield of snow crab (*Chionoecetes opilio*) off Tohoku, Japan via a state-space stock assessment model with time-varying natural mortality. Popul Ecol 63:41–60

Shimizu Y, Ito S (1996) A new method to draw isotherms in the Tohoku [Japan] offshore area: new interpolation method 'flexible Gaussian filter'. Bull Tohoku Natl Fish Res Inst 58:105–117 (in Japanese with English Abstract)

Stefanescu C, Rucabado J, Lloris D (1992) Depth-size trends in western Mediterranean demersal deep-sea fishes. Mar Ecol Prog Ser 81:205–213

Stevenson DE (2015) The validity of nominal species of *Malacocottus* (Teleostei: Cottiformes: Psychrolutidae)

known from the Eastern North Pacific with a key to the species. Copeia 103:22–33

Tian Y, Kidokoro H, Fujino T (2011) Interannual-decadal variability of demersal fish assemblages in the Tsushima Warm Current region of the Japan Sea: impacts of climate regime shifts and trawl fisheries with implications for ecosystem-based management. Fish Res 112:140–153

Tian Y, Nashida K, Sakaji H (2013) Synchrony in the abundance trend of spear squid *Loligo bleekeri* in the Japan Sea and the Pacific Ocean with special reference to the latitudinal differences in response to the climate regime shift. J Mar Sci 70:968–979

Wada T, Nemoto Y, Shimamura S, Fujita T and others (2013) Effects of the nuclear disaster on marine products in Fukushima. J Environ Radioact 124:246–254

Wada T, Fujita T, Nemoto Y, Shimamura S and others (2016) Effects of the nuclear disaster on marine products in Fukushima: an update after five years. J Environ Radioact 164:312–324

Wagawa T, Tamate T, Kuroda H, Ito S, Kakehi S, Yamanome T, Kodama T (2016) Relationship between coastal water properties and adult return of chum salmon (*Oncorhynchus keta*) along the Sanriku coast, Japan. Fish Oceanogr 25:598–609

Weinert M, Mathis M, Kroencke I, Neumann H, Pohlmann T, Reiss H (2016) Modelling climate change effects on benthos: distributional shifts in the North Sea from 2001 to 2099. Estuar Coast Shelf Sci 175:157–168

Yagura A (2021) Catches and ecology of gazami crab (*Portunus trituberculatus*) in Sendai Bay. Bull Miyagi Prefect Fish Technol Inst 21:9–14 (in Japanese)

Yamada U, Yagishita N (2013) Triglidae. In: Nakabo T (ed) Fishes of Japan with pictorial keys to the species, 3rd edn. Tokai University Press, Hadano p 720–726 (in Japanese)

Editorial responsibility: Konstantinos Stergiou, Thessaloniki, Greece
Reviewed by: B. Wolfe, N. D. Gallo and 1 anonymous referee

Submitted: March 11, 2021
Accepted: August 2, 2021
Proofs received from author(s): October 9, 2021